NANO · MICRO small
www.small-journal.com

Keeping Superprotonic Conductivity over a Wide Temperature Region via Sulfate Hopping Sites-Decorated Zirconium-Oxo Clusters

Wei-Lian Xie, Xiao-Min Li, Jiao-Min Lin, Long-zhang Dong, Yu Chen, Ning Li, Jing-Wen Shi, Jing-Jing Liu, Jiang Liu,* Shun-Li Li, and Ya-Qian Lan**

Metal-oxo clusters have emerged as advanced proton conductors with well-defined and tunable structures. Nevertheless, the exploitation of metal-oxo clusters with high and stable proton conductivity over a relatively wide temperature range still remains a great challenge. Herein, three sulfate groups decorated zirconium-oxo clusters (Zr_6, Zr_{18}, and Zr_{70}) as proton conductors are reported, which exhibit ultrahigh bulk proton conductivities of 1.71×10^{-1}, 2.01×10^{-2}, and 3.73×10^{-2} S cm^{-1} under 70 °C and 98% relative humidity (RH), respectively. Remarkably, Zr_6 and Zr_{70} with multiple sulfate groups as proton hopping sites show ultralow activation energies of 0.22 and 0.18 eV, respectively, and stable bulk conductivities of >10^{-2} S cm^{-1} between 30 and 70 °C at 98% RH. Moreover, a time-dependent proton conductivity test reveals that the best performing Zr_6 can maintain high proton conductivity up to 15 h with negligible loss at 70 °C and 98% RH, representing one of the best crystalline cluster-based proton conducting materials.

1. Introduction

Due to the efficient energy conversion and ultralow emission, proton-exchange membrane (PEM) fuel cells have attracted continuous attention in many fields, such as transportation and portable battery.[1] The explore of PEM materials with high and stable proton conductivity over a wide temperature range are of great significance for the operation of PEM fuel cells.[2] Currently, the most widely used PEM materials are perfluorinated polymers (e.g., Nafion), which have high proton conductivities (10^{-2}–10^{-1} s cm^{-1}) and reusability without significant performance decay.[3] Nevertheless, perfluorinated polymers usually involve complex synthesis process. Besides, they are amorphous polymers without clear structures, which make it challenging to uncover their proton transport mechanism for directionally improving the proton conducting performances.[4]

Recently, crystalline porous materials such as metal-organic frameworks (MOFs) and metal-oxo clusters have been extensively investigated in the pursuit of new proton conductors.[5] In particular, porous MOFs have attracted great attention because of their diverse structures and high porosity. Besides, their proton conducting performances can be effectively improved through structural functionalization, such as decorating functionalized groups (e.g., $-SO_3H$, $-COOH$, and $-PO_3H_2$) on the linkers or adding proton carriers (e.g., imidazole and sulfuric acid) into the porous channels.[6] Nevertheless, many porous MOFs are sensitive to water and easily to lose guest/water molecules, especially under high temperature, which make a great challenge for their application under these conditions.[7] Compared with MOFs, crystalline metal-oxo clusters, especially those constructed by high valence metal ions and O-contained ligands (e.g., SO_4^{2-} and PO_4^{2-}) usually show more stable in aqueous media.[8] In addition, their hydrophilic O-rich surface can function as proton hopping sites and binding sites

W.-L. Xie, J.-W. Shi
Jiangsu Collaborative Innovation Centre of Biomedical Functional Materials
Jiangsu Key Laboratory of New Power Batteries
School of Chemistry and Materials Science
Nanjing Normal University
Nanjing 210023, P. R. China

X.-M. Li
School of Materials Science and Engineering
Institute of Functional Porous Materials
Zhejiang Sci-Tech University
Hangzhou 310018, P. R. China

J.-M. Lin, L.-z. Dong, Y. Chen, J.-J. Liu, J. Liu, S.-L. Li, Y.-Q. Lan
School of Chemistry
South China Normal University
Guangzhou 510006, P. R. China
E-mail: linjm@m.scnu.edu.cn; liuj0828@m.scnu.edu.cn; yqlan@m.scnu.edu.cn

N. Li
School of Chemical Engineering and Light Industry
Guangdong University of Technology
Guangzhou, Guangdong 510006, P. R. China

The ORCID identification number(s) for the author(s) of this article can be found under https://doi.org/10.1002/smll.202205444.

DOI: 10.1002/smll.202205444

for proton transfer through forming effective hydrogen-bonded networks with guest/water molecules. Moreover, metal-oxo clusters with well-defined crystalline structures allow us to investigate their proton-conducting pathways and mechanisms at the molecular level.[9] Therefore, great research attentions in recent years have been devoted to develop metal-oxo cluster-based proton conductors. Many representative examples, especially polyoxometalate (POMs) based-proton conductors, have been achieved via different self-assembly strategies.[10] However, metal-oxo clusters that have high and stable proton conductivity (up to 10^{-2} s cm^{-1}) over a relatively wide temperature range are still not reported by far.

Zr-oxo clusters, as another important branch of metal-oxo clusters, have been widely investigated in catalysis and adsorption, but their proton conducting performances are still rare reported.[11] Indeed, Zr-oxo clusters with plenty of surface oxygens, strong Lewis acidity and high physicochemical stability have great potential for application in the field of proton conductor. In this work, the proton conducting performances of three sulfate (SO_4^{2-}) decorated zirconium-oxo clusters were studied for the first time. The utilization of sulfate groups as ligand here is based on the following considerations. Firstly, it has strong coordination ability with high-valence Zr^{4+} ions, which is helpful for the construction of large Zr-oxo clusters with high stability and insolubility in aqueous media.[12] Secondly, sulfate usually uses its two or three O atoms to coordinate with metal ions, leaving the other un-coordinated O atoms on the structural surface, which may be serve as proton hopping sites and form hydrogen-bonded networks with guest/water molecules for proton transfer.[13] Besides, owing to the stronger Lewis acidity of sulfate, the proton transfer on the O sites of sulfate may be more easily than that on the terminal coordinated O sites of the metal ions. Considering the above advantages, three sulfate groups decorated zirconium-oxo clusters, including $(Me_2NH_2)_4[Zr_6(SO_4)_6(\mu_3\text{-}O)_3(HTHAM)_3(CH_3O)_4]\cdot$ *N,N*-Dimethylformamide (DMF)$\cdot H_2O$ (**Zr$_6$**), (H_3THAM = tris(hydroxymethyl)aminomethane) $[Zr_{18}(SO_4)_{13}(O/OH/H_2O)_{56}]\cdot xH_2O$ (**Zr$_{18}$**) and $Zr_{70}(SO_4)_{58}(O/OH)_{146}\cdot x(H_2O)\cdot[Mg(H_2O)_6]_y$ (**Zr$_{70}$**), were synthesized and their proton conducting performances were investigated for the first time. As expected, **Zr$_6$**, **Zr$_{18}$** and **Zr$_{70}$** exhibit ultrahigh bulk conductivities of 1.71×10^{-1}, 2.01×10^{-2}, and 3.73×10^{-2} S cm^{-1} under 70 °C and 98% relative humidity (RH), respectively, which are comparable to that of the best-performing metal-oxo cluster-based proton conductors under analogous conditions. The total conductivities of **Zr$_6$**, **Zr$_{18}$** and **Zr$_{70}$** at this temperature and RH were calculated to be 6.73×10^{-2}, 6.64×10^{-4}, and 5.24×10^{-3} S cm^{-1}, respectively. Additionally, owing to the multiple sulfate groups decorated on the zirconium-oxo cluster surface that can act as proton hopping and transfer sites, **Zr$_6$** and **Zr$_{70}$** show ultralow activation energy of 0.22 and 0.18 eV, respectively. Furthermore, the bulk proton conductivities of **Zr$_6$** and **Zr$_{70}$** were found to be less dependent on the temperature (6.90×10^{-2}–1.71×10^{-1} S cm^{-1} for **Zr$_6$** and 1.90×10^{-2}–3.73×10^{-2} S cm^{-1} for **Zr$_{70}$** under temperature between 30 and 70 °C at 98% RH), which is the first observed among metal-oxo cluster-based proton conductors. Besides, time-dependent proton conductivity test revealed that **Zr$_6$** with the best performance can maintain high proton conductivity up to 15 h without obvious loss, suggesting it has great potential for further application in PEM.

2. Results and Discussion

Colorless crystals of **Zr$_6$**, **Zr$_{18}$**, and **Zr$_{70}$** were synthesized through solvothermal reaction (for details, see the Experimental Section). Single-crystal X-ray diffraction analysis revealed that **Zr$_6$** is a new hexa-nuclear cluster (**Figure 1**a,b), crystalizing in the orthorhombic space group *Pnma* (Table S1, Supporting Information). The asymmetric unit of **Zr$_6$** involves four crystallographically independent Zr atoms (Zr1, Zr2, Zr3, and Zr4), three SO_4^{2-}, sesqui $HTHAM^{2-}$ ligands, sesqui μ_3-O atoms, two $-OCH_3$ groups, one guest water molecule, a half of free DMF molecule, and two dimethylamine counter cations (Figure S1, Supporting Information). In **Zr$_6$**, Zr1, and Zr3 atoms are seven coordination and exhibit distorted pentagonal bipyramid geometry, while Zr2 and Zr4 atoms are eight coordination and possess distorted dodecahedron geometry (Figure S2, Supporting Information). Zr1 and Zr3 have similar coordination environment, in which each Zr ions coordinates with seven O atoms from two SO_4^{2-}, two $HTHAM^{2-}$ ligands, one $-OCH_3$ group, and one μ_3-O atom. Zr2 and Zr4 also exhibit similar coordination environment with each Zr ion coordinated by one N and seven O atoms from one $HTHAM^{2-}$ ligand, two SO_4^{2-}, two μ_3-O and one μ_3-OCH_3 group. Six Zr ions are linked together by three μ_3-O and one μ_3-OCH_3 groups to from a hexa-nuclear Zr-oxo core with tripod-shaped geometry. The outer coordination space of this Zr-oxo core is surrounded by six SO_4^{2-}, three $HTHAM^{2-}$ ligands, and three $-OCH_3$ groups. Interesting, the $HTHAM^{2-}$ and SO_4^{2-} ligands in **Zr$_6$** used μ_3-η^2:η^2:η^1:η^0 (tridentate) and μ_3-η^1:η^1:η^1:η^0 (tridentate)/μ_2-η^1:η^1:η^0:η^0 (bidentate) coordination modes, respectively, leaving one hydroxyl group and one or two O atoms to be uncoordinated, which form hydrogen bond interactions with surrounding molecules, such as dimethylamine cations, DMF and water molecules (O...N, 2.848–2.916 Å; O...O, 2.850–2.958 Å) (Table S3, Supporting Information). The hexa-nuclear clusters and guest molecules are packed together spontaneously and orderly to form a 3D supramolecular structure (Figure 1c).

Zr$_{18}$ is an eighteen-nuclear zirconium cluster whose Zr-oxo core is decorated by 13 SO_4^{2-} ligands (Figure 1d). Notably, there are also two types of coordination modes for the SO_4^{2-} ligands in **Zr$_{18}$**. Type I, each SO_4^{2-} ligand coordinates with three Zr atoms in a tridentate fashion; and type II, each SO_4^{2-} ligand chelates one Zr atom or coordinates with two Zr atoms in bidentate fashion. The adjacent **Zr$_{18}$** clusters are bridged together by bidentate SO_4^{2-} to form 1D chains (Figure 1e), which further stack together to construct a 3D supramolecular structure with small channels (Figure S3, Supporting Information). Guest water molecules in the channels form effective hydrogen bonds with the oxygen atoms on the SO_4^{2-} and the Zr-oxo core. **Zr$_{70}$** is a toroidal oxysulfate cluster with an inner cavity of about 1 nm. The edges of both inner and outer ring of **Zr$_{70}$** are covered by 56 SO_4^{2-} ligands (Figure 1f), for which 20 SO_4^{2-} in the inner rim connect to 50 Zr atoms in tridentate coordination mode, and 36 SO_4^{2-} in the outer rim connect to 60 Zr atoms in bidentate or tridentate coordination modes.

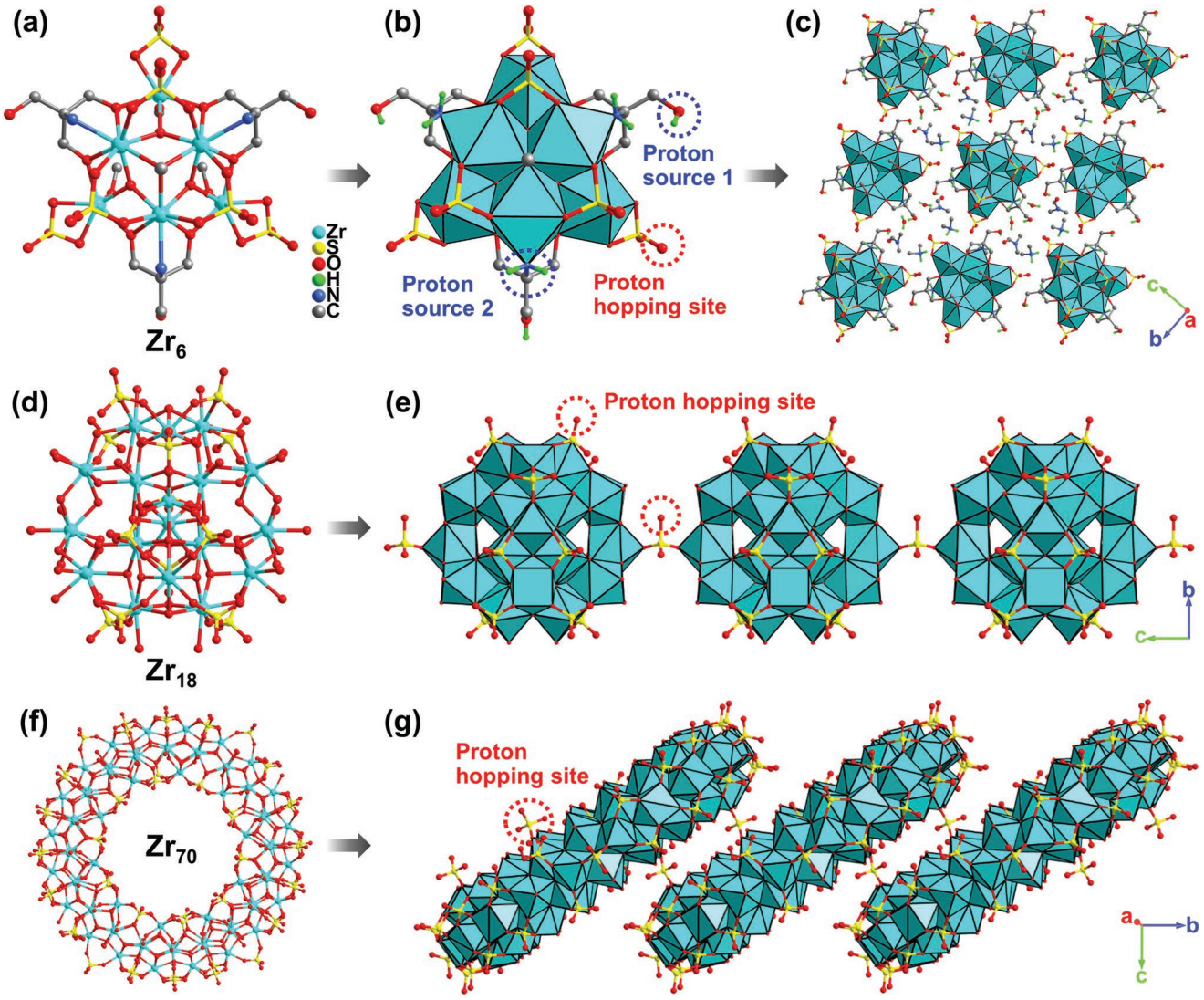

Figure 1. Crystal structures of Zr_6, Zr_{18}, and Zr_{70}. a) Ball-and-stick representation of Zr_6. b) Polyhedral and ball-and-stick representation of Zr_6. c) 3D supramolecular stacking of Zr_6. d) Ball-and-stick representation of Zr_{18}. e) The 1D chain of Zr_{18} in polyhedral and ball-and-stick representation. f) Ball-and-stick representation of Zr_{70}. g) The 1D chain of Zr_{70} in polyhedral and ball-and-stick representation. Zr: turquoise; S: yellow; O: red; N: blue; H: green; C: gray.

Therefore, there are also abundant uncoordinated sulfate O atoms on the surface of this cluster, which can be utilized as potential proton hopping sites. Each toroidal cluster connects with two other clusters by two bridging SO_4^{2-} to form staircase-like chains (Figure 1g and Figure S4, Supporting Information), which further parallel stacking together in a herringbone-like mode to construct a 3D supramolecular structure with small channels (Figure S5, Supporting Information). Similarly, guest water molecules and magnesium counter cations (coordinated by six water molecules) in the channels form multiple hydrogen bonds with the main framework to construct effective hydrogen-bonded network for proton transfer.

The experimental powder X-ray diffraction (PXRD) patterns of Zr_6, Zr_{18}, and Zr_{70} are in good agreement with that of the simulated results from their single crystal structures, indicating that they possess high purity (Figures S6–S8, Supporting Information). To further characterize the compositions of Zr_6, Zr_{18}, and Zr_{70}, the Fourier transform infrared (FTIR) spectroscopy measurement was performed. As shown in Figure S9 in the Supporting Information, the strong and broad band at about 3421 cm^{-1} and the band at about 1630 cm^{-1} are associated with the O—H stretching and bending vibration, respectively, which indicate that a large number of crystalline water molecules and hydrogen bonds may be existed in these Zr-oxo clusters.[14] The bands in the region of 900–1240 cm^{-1} ascribed to the asymmetric and symmetric stretching of the sulfate ligands.[15] Furthermore, the X-ray photoelectron spectroscopy (XPS) spectrum of Zr_6 was determined to analyze the composition and the valence state of the Zr ion, which demonstrated the presence of Zr, O, S, C, and N elements in this compound (Figure S10, Supporting Information). The peaks at 182.5 and 185 eV correspond to the binding energies of $Zr3d_{5/2}$

and $Zr3d_{3/2}$, respectively, indicating that the valence state of Zr ion in $\mathbf{Zr_6}$ is +IV.[16] To evaluate their thermal stability, the thermogravimetric analysis (TGA) were performed at 25–900 °C under nitrogen atmosphere. As shown in Figure S11 in the Supporting Information, the thermogravimetric curve of $\mathbf{Zr_6}$ shows a weight loss of 9.1% below 100 °C and another small weight loss of 5% at 100–210 °C, which correspond to the loss of guest water molecules, dimethylamine cations and DMF. The structure of $\mathbf{Zr_6}$ maintains up to about 300 °C. As for $\mathbf{Zr_{18}}$ and $\mathbf{Zr_{70}}$, initial weight loss was observed from room temperature to 150 °C, which corresponds to the release of lattice and coordinated water molecules. Subsequently, they keep structure stable until the removal of the sulfate ligands at about 660 °C, suggesting good thermal stability of these zirconium-oxo clusters.

Considering the existence of multiple sulfate proton hopping sites and extensive hydrogen-bonded networks in $\mathbf{Zr_6}$, $\mathbf{Zr_{18}}$, and $\mathbf{Zr_{70}}$, they are encouraged to be good candidates of proton conductors. To assess their proton conducting performance, alternating current impedance spectroscopy measurements using compacted pellets of the powdered crystalline samples were conducted under 40–98% RH at 30 °C. The impedance spectra of $\mathbf{Zr_6}$, $\mathbf{Zr_{18}}$, and $\mathbf{Zr_{70}}$ are shown in **Figure 2**a–c and their bulk and total proton conductivities were determined from the semicircles in the Nyquist plots. The semicircle in the high-frequency region relates to the bulk and grain boundary resistances, and the tail in the low-frequency region corresponds to the mobile ions, which are blocked by the interface between electrode and electrolyte.[17] The results revealed that the bulk proton conductivities of $\mathbf{Zr_6}$, $\mathbf{Zr_{18}}$, and $\mathbf{Zr_{70}}$ increase rapidly with the increase of humidity and reached 6.90×10^{-2}, 2.62×10^{-3}, and 1.90×10^{-2} S cm^{-1} at 30 °C and 98% RH, respectively (Figures S12–S14, Supporting Information). Noted that the bulk conductivities of $\mathbf{Zr_6}$ and $\mathbf{Zr_{70}}$ at this temperature and RH are within the range of superprotonic conductivity and are higher than most known metal-oxo cluster-based proton conductors under analogous conditions (for metal-oxo cluster-based proton conductors, only our recently reported polymolybdate cluster Mo_{240} with proton conductivity >10^{-2} S cm^{-1} at 25 °C).[18] The high photon conducting performance of $\mathbf{Zr_6}$ and $\mathbf{Zr_{70}}$ at low temperature should be attributed to the multiple sulfate groups on their structural surface that can not only act as proton hopping sites but also easily form extensive hydrogen-bonded networks with guest and adsorbed water molecules for promoting proton transport. To verify their humidity dependent proton conducting properties, water vapor absorption and desorption isotherms were measured at 298 K. As shown in Figure 2d, the water vapor adsorption of $\mathbf{Zr_6}$, $\mathbf{Zr_{18}}$, and $\mathbf{Zr_{70}}$ increase with the increasing humidity, which are consistent with the change of proton conductivity, suggesting they are humidity dependent proton conductors. Besides, under high humidity, the highest water vapor uptake of $\mathbf{Zr_6}$, $\mathbf{Zr_{18}}$, and $\mathbf{Zr_{70}}$ can reach 286.7, 131.2, and 432.8 cm^3 g^{-1}, respectively, indicating they have high hydrophilia, which should be due to the existence of abundant sulfate groups that can easily form strong hydrogen bonds with adsorbed water molecules, and thus promote their proton conducting performances.

The proton conductivities of $\mathbf{Zr_6}$, $\mathbf{Zr_{18}}$, and $\mathbf{Zr_{70}}$ were further investigated at 30–70 °C under a constant RH of 98%. Interestingly, with the temperature increase from 30 to 70 °C, the bulk conductivity of $\mathbf{Zr_6}$ and $\mathbf{Zr_{70}}$ increase very slowly from

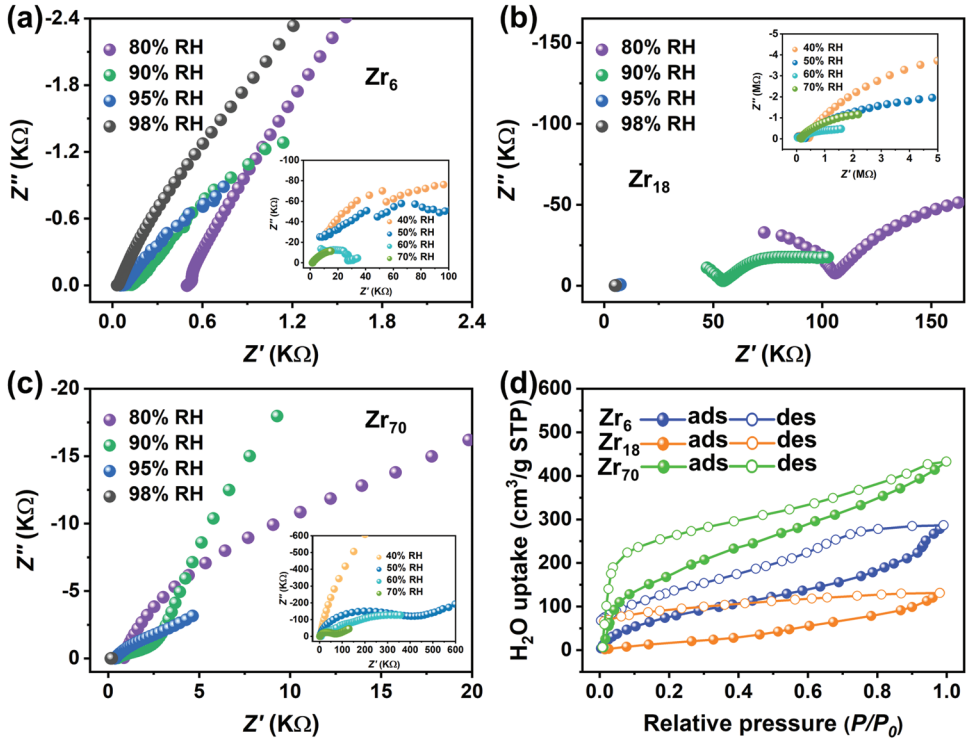

Figure 2. The Nyquist plots of a) $\mathbf{Zr_6}$, b) $\mathbf{Zr_{18}}$, and c) $\mathbf{Zr_{70}}$ at 30 °C and various humidity variations from 40% to 98%. d) The water vapor adsorption and desorption isotherms of $\mathbf{Zr_6}$, $\mathbf{Zr_{18}}$, and $\mathbf{Zr_{70}}$ at 298 K.

6.90×10^{-2} to 1.71×10^{-1} and 1.90×10^{-2} to 3.73×10^{-2} S cm^{-1}, respectively, showing less temperature dependent proton conductivity, while that of **Zr$_{18}$** increase obviously from 2.62×10^{-3} to 2.01×10^{-2} S cm^{-1}, showing typical temperature dependent proton conductivity (**Figure 3**a,b and Figures S15 and S16, Supporting Information). Noted that proton conductors with high and stable proton conductivity over a relatively wide temperature range are of great significance for practical application since they may work in different temperatures. Nevertheless, current reported metal-oxo cluster-based proton conductors with such attracted properties are still very limit. To the best of our knowledge, **Zr$_6$** and **Zr$_{70}$** represent the first examples of metal-oxo clusters that possessed high and stable bulk proton conductivities of $>10^{-2}$ S cm^{-1} over a relatively wide temperature range from 30 to 70 °C. In addition, **Zr$_6$** shows proton conductivity up to 1.71×10^{-1} S cm^{-1} at 70 °C and 98% RH, which is one of the highest among metal-oxo cluster-based proton conductors and is comparable to that of the best-performing MOF materials reported by far (Figure 3d and Table S4, Supporting Information). The total proton conductivities of **Zr$_6$**, **Zr$_{18}$**, and **Zr$_{70}$** were determined to be 6.73×10^{-2}, 6.64×10^{-4}, and 5.24×10^{-3} S cm^{-1} at 70 °C and 98% RH, respectively (Table S5, Supporting Information). To gain insight into their proton transfer mechanisms, the activation energies (E_a) of **Zr$_6$**, **Zr$_{18}$**, and **Zr$_{70}$** at 98% RH and 30–70 °C were calculated according to the Arrhenius equation (Figure 3c). The results revealed that **Zr$_{18}$** shows an E_a of 0.50 eV, suggesting that the dominated proton conduction mechanism for this compound is vehicle mechanism (accomplishes proton transport by diffusive routes, generally with $E_a > 0.4$ eV).[19] In contrast, **Zr$_6$** and **Zr$_{70}$** exhibit ultralow E_a of 0.22 and 0.18 eV, respectively, indicating their dominated proton conduction mechanisms are Grotthuss mechanism (establishes proton pathway via hydrogen-bonded networks, generally with $E_a < 0.4$ eV).[20] It is worth noting that the E_a of **Zr$_6$** and **Zr$_{70}$** belong to ultralow values among metal-oxo cluster-based proton conductors reported to date (Figure 3d and Table S4, Supporting Information). The low E_a of **Zr$_6$** and **Zr$_{70}$** are consistent with their high and stable proton conductivities, suggesting that the proton transfer in these two compounds is fast and efficient, which should be due to the present of multiple sulfate proton hopping sites and extensive hydrogen-bonded networks within their structures.

The performance stability of proton conductors is the basis for their further application. The proton conducting stability of **Zr$_6$**, **Zr$_{18}$**, and **Zr$_{70}$** were assessed under heating-cooling cycle (30–70 °C) at 98% RH. As shown in Figure 3e and Figures S17–S21 in the Supporting Information, the proton conductivities in their heating process are basically consistent with that in their cooling process, suggesting that they possess good stability of proton conducting performance. In addition, there is almost no change for the activation energy during the heating–cooling cycle, which indicates that the proton transport mechanisms of these compounds are sustainable (Figures S22–S24, Supporting Information). Moreover, time-dependent proton conductivity test was performed on best performing **Zr$_6$** at 70 °C and 98% RH to evaluate its durability. As shown in Figure 3f, the proton conductivity of **Zr$_6$** can maintain up to 15 h with only a negligible loss, suggesting good proton conducting durability of this compound. In addition, the structural integrity of **Zr$_{18}$** and **Zr$_{70}$** are well maintained after the impedance test, as confirmed

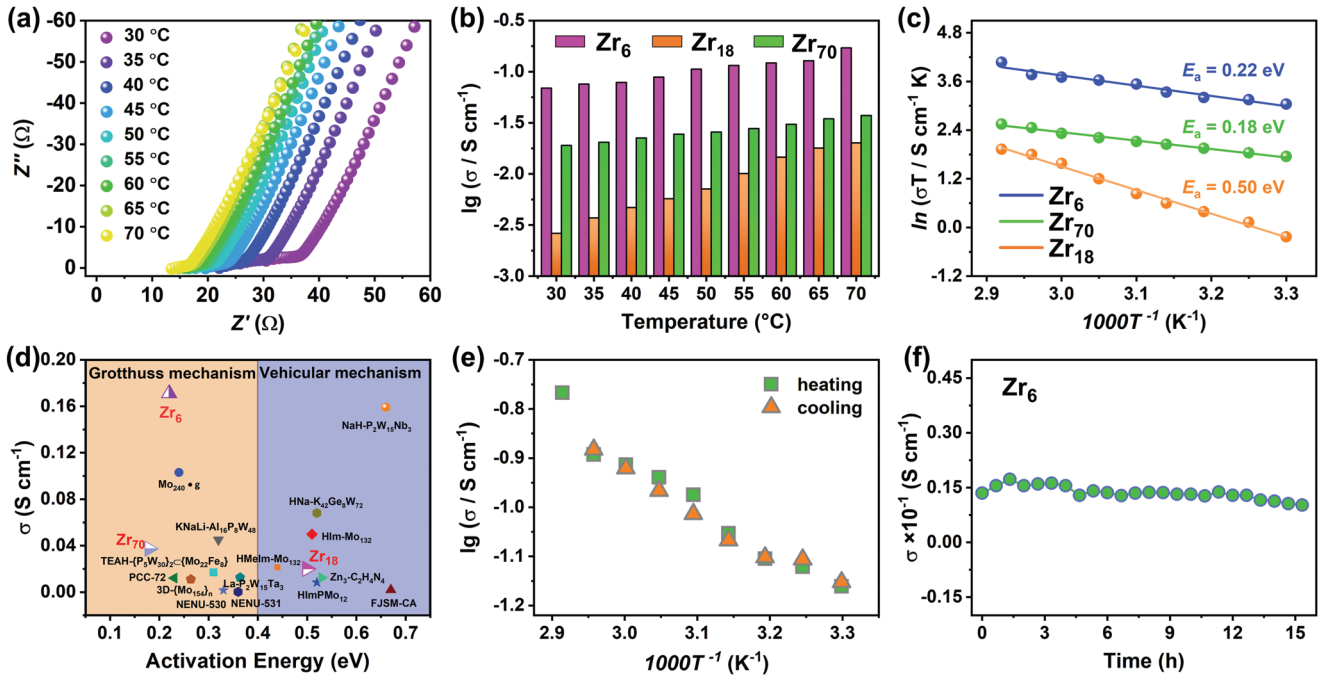

Figure 3. a) The Nyquist plots of **Zr$_6$** at 98% RH and various temperature variations from 30 to 70 °C. b) Bulk proton conductivities of **Zr$_6$** (pink), **Zr$_{18}$** (orange) and **Zr$_{70}$** (green) with temperature variations from 30 to 70 °C at 98% RH. c) Arrhenius plots of **Zr$_6$** (blue), **Zr$_{18}$** (orange) and **Zr$_{70}$** (green) under 98% RH and different temperature variations from 30 to 70 °C. d) Comparison of the bulk proton conductivities and activation energies of **Zr$_6$**, **Zr$_{18}$**, **Zr$_{70}$** and some representative metal-oxo based proton conductors under similar conditions. e) Bulk proton conductivity for the heating-cooling cycle of **Zr$_6$** at 98% RH and temperature range of 30–70 °C. f) Time-dependent bulk conductivity of **Zr$_6$** measured at 70 °C and 98% RH.

by the PXRD and FTIR (Figures S26, S27, S29, and S30, Supporting Information). Nevertheless, the PXRD pattern of **Zr_6** showed slight shift after the impedance test, indicating that it had slight structure change but remained crystallinity, which may be due to the change/shift of guest molecules during the impedance test and thus leading to the change/shift of their molecular packing. The FTIR spectra of **Zr_6** before and after impedance measurement have no obvious change, suggesting its main structure remained intact during impedance analyses (Figures S25 and S28, Supporting Information).

It is interesting that although **Zr_6**, **Zr_{18}**, and **Zr_{70}** are all decorated with coordinated sulfate groups as hopping sites, they exhibit significantly different proton conducting performances and E_a. To understand these differences, we carefully analyzed their host–guest interactions from their crystal structures. As shown in **Figure 4**a, in **Zr6**, excepting sulfate groups, there are many other N- and O-contained hydrophilic groups, such as $HTHAM^{2-}$, DMF, and $Me_2NH_2^+$ counter cations, can participate in the construction of the hydrogen-bonded network with adsorbed water molecules.[21] Therefore, for **Zr6**, the formation of dense hydrogen-bonded network for proton hopping and transfer are much easy, and thus resulting ultralow E_a and ultrahigh proton conductivity over a relatively wide temperature range at high RH. While for **Zr_{70}**, its both inner and outer Zr-oxo ring are covered by multiple coordinated sulfate groups, which make it easy to form strong hydrogen bonds with adsorbed water molecules, as confirmed by its high water uptake capacity in the low P/P_0 region of the water vapor adsorption isotherm (Figure 2d). Therefore, it is also easy for **Zr_{70}** to form effective hydrogen-bonded network for proton transfer under high RH (Figure 4c). Thus, **Zr_{70}** exhibits high proton conductivity with low E_a at high RH, even under low temperature; but shows low proton conductivity at low RH. Compared with **Zr_6** and **Zr_{70}**, the arrangement of sulfate groups on the surface of **Zr_{18}** is more random and sparse, which may make it more difficult to construct effective hydrogen-bonded network for proton transfer (Figure 4b). Besides, there is no other additional hydrophilic ligands or guest molecules (excepted water) that can assistant the formation of hydrogen bonds with water molecules for this compound, as demonstrated by its weak water uptake capacity (Figure 2d). Thus, **Zr_{18}** exhibits relatively poorer proton conductivity and higher E_a as compared with that of **Zr_6** and **Zr_{70}**. Therefore, excepting the introduction of functional groups, their spatial arrangement is also crucial important for the construction of dense hydrogen-bonded networks for effective proton hopping and transfer.

3. Conclusion

In summary, we have successfully prepared three sulfate hopping sites-decorated Zr-oxo clusters as proton conductors for the first time, which are **Zr_6**, **Zr_{18}**, and **Zr_{70}**. Specifically, under 70 °C and 98% RH, **Zr_6** and **Zr_{70}** exhibit outstanding bulk conductivities of 1.71×10^{-1} S cm^{-1} and 3.73×10^{-2} S cm^{-1} with ultralow low E_a of 0.22 and 0.18 eV, respectively. Besides, owing to the multiple coordinated sulfate groups that can act as proton hopping sites and simultaneously promote the construction of extensive hydrogen-bonded networks with adsorbed water molecules for effective proton transfer, **Zr_6** and **Zr_{70}** display stable proton conductivities of $>10^{-2}$ S cm^{-1} over a relatively wide temperature range (from 30 to 70 °C) at 98% RH, which is the first observed among metal-oxo cluster-based proton conductors. By contrast, **Zr_{18}** shows relatively poor proton conductivity and high E_a since the decorated sulfate groups in this compound are relatively random and sparse, as compared with that of **Zr_6** and **Zr_{70}**. This work provides an important example for the development of Zr-oxo cluster-based proton conductors with high and stable proton conductivity over a relatively wide temperature range through effectively utilized coordinated sulfate groups.

4. Experimental Section

Preparation of Materials: All starting materials and reagents used in experiments were commercially available and used without further purification. All solutions used in experiments were prepared with Millipore water (18.25 MΩ). Zirconium propoxide solution ($C_{12}H_{28}O_4Zr$, 70 wt%) was purchased from Aladdin. Concentrated sulfuric acid (H_2SO_4, 95%-98%), zirconium oxychloride octahydrate ($ZrOCl_2{\cdot}8H_2O$, ≥ 99%), and magnesium nitrate hexahydrate ($Mg(NO_3)_2{\cdot}6H_2O$) were purchased from Sinopharm Chemical Reagent Co. Ltd. Ammonium sulfate ($(NH_4)_2SO_4$, ≥ 99%) was purchased from Shanghai Lingfeng Chemical Reagents Co. Ltd. DMF (≥ 99.8%) and methyl alcohol (CH_3OH, ≥ 99.5%) were purchased from General-reagent. Zirconium sulfate tetrahydrate ($Zr(SO_4)_2{\cdot}4H_2O$, 98%+) and tris(hydroxymethyl) aminomethane (H_3THAM, 99%) were purchased from Adamas-beta.

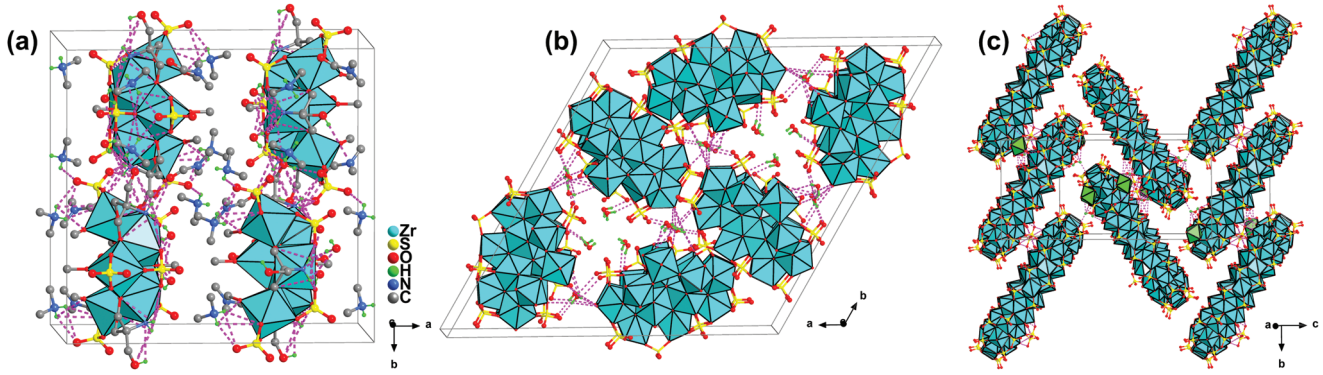

Figure 4. Schematic view of possible proton transport pathways in a) **Zr6**, b) **Zr18**, and c) **Zr70**. Pink lines represent hydrogen bonds. Polyhedral color code: MgO_6, green.

Synthesis of **Zr_6**: Tris(hydroxymethyl) aminomethane (0.012 g, 0.1 mmol) and zirconium propoxide solution (0.25 mL, 0.8 mmol) were dissolved in a mixed solution of DMF/MeOH (5 mL, 1:1, v/v) under stirring for about 10 min, and then followed by the addition of five drops of sulfuric acid (0.046 mL, 0.87 mmol). The colorless solution was transferred into a 10 mL glass bottle and heated to 85 °C in constant temperature oven for 3 d. After cooling down to room temperature, colorless rhomboid block crystals were collected by filtration and fully washed several times with the mixture of DMF/MeOH (1:1, v/v). Yield: 84%.

Synthesis of **Zr_{18}**: It was synthesized according to literature with a slightly change.[22] In detail, zirconium oxychloride octahydrate (0.322 g, 1 mmol) and sulfuric acid (0.035 mL, 0.66 mmol) were dissolved in 2 mL of H_2O with stirring for about 10 min and then followed by the addition of ammonium sulfate solution (1 mL, 0.5 M). The colorless solution was transferred into a 10 mL glass bottle and heated to 90 °C for 4 d. After cooling down to room temperature, colorless needle-like crystals were collected and fully washed several times with water.

Synthesis of **Zr_{70}**: It was synthesized according to the reported literature.[23]

Structural Characterization: The room-temperature PXRD spectra were recorded ranging from 3° to 50° at room temperature on a Rigaku D/Max 2500/PC diffractometer at 40 kV and 100 mA with a Cu-target tube and a graphite monochromator. TGA of the samples were performed on a Diamond thermogravimetric analysis/differential thermal analysis/differential scanning calorimetry analyzer at a heating rate of 10 °C min^{-1} from ambient temperature to 900 °C under a nitrogen gas atmosphere. FTIR spectrum was measured on a Brucker Tensor 27 in the range of 4000–400 cm^{-1} using the technique of pressed KBr pellets. Water vapor adsorption and desorption isotherms were measured at 298 K on a BELSORP MAX instrument. XPS were recorded using Escalab 250Xi instrument (Thermo Fisher Scientific) equipped with an Al K_α microfocused X-ray source.

Single-Crystal X-Ray Diffraction Analyses: The diffraction data of **Zr_6** and **Zr_{18}** were collected on a Bruker AXS smart Apex II charge coupled device diffractometer at 150 and 296.15 K. The X-ray generator was operated at 50 kV and 35 A using Mo K_α (λ = 0.71073 Å) radiation. The crystal structures were solved and refined by full matrixcs methods against F^2 using SHELXL-2018[24] program package and Olex-2 software.[25] All nonhydrogen atoms were refined using anisotropic displacement parameters and the positions of hydrogen were fixed in the calculated positions and refined isotropically. The detailed structure determination parameters and crystallographic data of **Zr_6** and **Zr_{18}** are summarized in Table S1 in the Supporting Information. The selected bond lengths and angles of **Zr_6** are listed in Table S2 in the Supporting Information. CCDC 2182124 (**Zr_6**) contains the supplementary crystallographic data for the paper. These data can be obtained free of charge from the Cambridge Crystallographic Data Centre.

Proton Conductivity Characterization: First, the single crystals were uniformly ground into powder and then were put into a homemade mold with a radius of 0.2 cm to obtain circular pellets. The thickness was measured by a vernier caliper. And the thickness of **Zr_6**, **Zr_{18}** and **Zr_{70}** was 1.31, 2.40, and 1.80 mm, respectively. Second, both sides of the pellets were coated with silver glue and dried naturally in air. Third, the pellets were fixed on the sample stage with gold wires. The proton conductivities were measured using an impedance/gain-phase analyzer (Solartron S1 1260) with a quasi-four-probe method over a frequency range from 1 Hz to 1 MHz within the input voltage of 100 mV. The measurements were operated at 30 °C with different RHs (40–98%) and under 98% RH with various temperatures (30–70 °C). The impedances at each temperature were tested after equilibration for 30 min. The higher-frequency intercepts along the *x*-axes of the impedance plots were used to calculate the bulk resistance of the samples. And then the bulk resistance was used to calculate the conductivities of the samples. The values of proton conductivities were calculated by the following equation

$$\sigma = \frac{l}{SR} \tag{1}$$

where σ, l, S, and R represent the conductivity (S cm^{-1}), the thickness (cm) of the pellet, the cross-sectional area (cm^2) of the pellet, and the bulk resistance (Ω), respectively. The activation energy (E_a) was calculated using the following equation

$$\ln\sigma_T = \ln\sigma_0 - \frac{E_a}{KT} \tag{2}$$

$$K = 8.6 \times 10^{-5}\, eV\, K^{-1} \tag{3}$$

where σ is the conductivity (S cm^{-1}), K is the Boltzmann constant (eV K^{-1}), and T is the temperature (K).

Supporting Information

Supporting Information is available from the Wiley Online Library or from the author.

Acknowledgements

W.-L.X. and X.-M.L. contributed equally to this work. This work was financially supported by the National Natural Science Foundation of China (Nos. 92061101, 21871142, 21871141, 22071109, 22225109 and 22271104), the Excellent Youth Foundation of Jiangsu Natural Science Foundation (No. BK20211593), Priority Academic Program Development of Jiangsu Higher Education Institutions and Foundation of Jiangsu Collaborative Innovation Center of Biomedical Functional Materials.

Conflict of Interest

The authors declare no conflict of interest.

Data Availability Statement

The data that support the findings of this study are available from the corresponding author upon reasonable request.

Keywords

hydrogen bonds, Lewis acidity, proton transport, sulfate group, zirconium-oxo clusters

Received: September 3, 2022
Revised: September 24, 2022
Published online: October 25, 2022

[1] a) A. Kirubakaran, S. Jain, R. K. Nema, *Renewable Sustainable Energy Rev.* **2009**, *13*, 2430; b) M. Lopez-Haro, L. Guétaz, T. Printemps, A. Morin, S. Escribano, P. H. Jouneau, P. Bayle-Guillemaud, F. Chandezon, G. Gebel, *Nat. Commun.* **2014**, *5*, 5229; c) K. Jiao, J. Xuan, Q. Du, Z. Bao, B. Xie, B. Wang, Y. Zhao, L. Fan, H. Wang, Z. Hou, S. Huo, N. P. Brandon, Y. Yin, M. D. Guiver, *Nature* **2021**, *595*, 361; d) S. C. Pal, M. C. Das, *Adv. Funct. Mater.* **2021**, *31*, 2101584.
[2] Z. P. Cano, D. Banham, S. Ye, A. Hintennach, J. Lu, M. Fowler, Z. Chen, *Nat. Energy* **2018**, *3*, 279.
[3] a) V. Di Noto, M. Piga, G. A. Giffin, K. Vezzù, T. A. Zawodzinski, *J. Am. Chem. Soc.* **2012**, *134*, 19099; b) H. S. Sasmal, H. B. Aiyappa, S. N. Bhange, S. Karak, A. Halder, S. Kurungot, R. Banerjee, *Angew.*

Chem., Int. Ed. **2018**, *57*, 10894; c) D. W. Kang, M. Kang, C. S. Hong, *J. Mater. Chem. A* **2020**, *8*, 7474.

[4] a) H. Zhang, P. K. Shen, *Chem. Rev.* **2012**, *112*, 2780; b) X. Meng, H.-N. Wang, S.-Y. Song, H.-J. Zhang, *Chem. Soc. Rev.* **2017**, *46*, 464.

[5] a) M. Sadakiyo, T. Yamada, H. Kitagawa, *J. Am. Chem. Soc.* **2014**, *136*, 13166; b) K. Zhang, X. Xie, H. Li, J. Gao, L. Nie, Y. Pan, J. Xie, D. Tian, W. Liu, Q. Fan, H. Su, L. Huang, W. Huang, *Adv. Mater.* **2017**, *29*, 1701804; c) Z.-H. Li, H. Zeng, G. Zeng, C. Ru, G. Li, W. Yan, Z. Shi, S. Feng, *Angew. Chem., Int. Ed.* **2021**, *60*, 26577; d) S.-L. Yang, G. Li, M.-Y. Guo, W.-S. Liu, R. Bu, E.-Q. Gao, *J. Am. Chem. Soc.* **2021**, *143*, 8838; e) L. Qin, Y.-Z. Yu, P.-Q. Liao, W. Xue, Z. Zheng, X.-M. Chen, Y.-Z. Zheng, *Adv. Mater.* **2016**, *28*, 10772; f) Z. Li, X.-X. Li, T. Yang, Z.-W. Cai, S.-T. Zheng, *Angew. Chem., Int. Ed.* **2017**, *56*, 2664; g) J.-C. Liu, Q. Han, L.-J. Chen, J.-W. Zhao, C. Streb, Y.-F. Song, *Angew. Chem., Int. Ed.* **2018**, *57*, 8416; h) X.-M. Li, L.-Z. Dong, J. Liu, W.-X. Ji, S.-L. Li, Y.-Q. Lan, *Chem* **2020**, *6*, 2272.

[6] a) W. J. Phang, W. R. Lee, K. Yoo, D. W. Ryu, B. Kim, C. S. Hong, *Angew. Chem., Int. Ed.* **2014**, *53*, 8383; b) S. Pili, S. P. Argent, C. G. Morris, P. Rought, V. García-Sakai, I. P. Silverwood, T. L. Easun, M. Li, M. R. Warren, C. A. Murray, C. C. Tang, S. Yang, M. Schröder, *J. Am. Chem. Soc.* **2016**, *138*, 6352; c) F. Yang, G. Xu, Y. Dou, B. Wang, H. Zhang, H. Wu, W. Zhou, J.-R. Li, B. Chen, *Nat. Energy* **2017**, *2*, 877; d) Y. Ye, W. Guo, L. Wang, Z. Li, Z. Song, J. Chen, Z. Zhang, S. Xiang, B. Chen, *J. Am. Chem. Soc.* **2017**, *139*, 15604; e) S. Kim, B. Joarder, J. A. Hurd, J. Zhang, K. W. Dawson, B. S. Gelfand, N. E. Wong, G. K. H. Shimizu, *J. Am. Chem. Soc.* **2018**, *140*, 1077; f) M. K. Sarango-Ramírez, J. Park, J. Kim, Y. Yoshida, D.-W. Lim, H. Kitagawa, *Angew. Chem., Int. Ed.* **2021**, *60*, 20173.

[7] a) J. A. Greathouse, M. D. Allendorf, *J. Am. Chem. Soc.* **2006**, *128*, 10678; b) S. Tominaka, F.-X. Coudert, T. D. Dao, T. Nagao, A. K. Cheetham, *J. Am. Chem. Soc.* **2015**, *137*, 6428.

[8] a) G.-H. Chen, Y.-P. He, S.-H. Zhang, L. Zhang, *Inorg. Chem. Commun.* **2018**, *97*, 125; b) I. Colliard, M. Nyman, *Angew. Chem., Int. Ed.* **2021**, *60*, 7308.

[9] a) S. Zhang, Y. Lu, X.-W. Sun, Z. Li, T.-Y. Dang, Z. Zhang, H.-R. Tian, S.-X. Liu, *Chem. Commun.* **2020**, *56*, 391; b) T. Iwano, K. Shitamatsu, N. Ogiwara, M. Okuno, Y. Kikukawa, S. Ikemoto, S. Shirai, S. Muratsugu, P. G. Waddell, R. J. Errington, M. Sadakane, S. Uchida, *ACS Appl. Mater. Interfaces* **2021**, *13*, 19138.

[10] a) P. Yang, M. Alsufyani, A.-H. Emwas, C. Chen, N. M. Khashab, *Angew. Chem., Int. Ed.* **2018**, *57*, 13046; b) S. Li, Y. Zhao, S. Knoll, R. Liu, G. Li, Q. Peng, P. Qiu, D. He, C. Streb, X. Chen, *Angew. Chem., Int. Ed.* **2021**, *60*, 16953; c) S.-R. Li, H.-Y. Wang, H.-F. Su, H.-J. Chen, M.-H. Du, L.-S. Long, X.-J. Kong, L.-S. Zheng, *Small Methods* **2021**, *5*, 2000777; d) M. Zhu, T. Iwano, M. Tan, D. Akutsu, S. Uchida, G. Chen, X. Fang, *Angew. Chem., Int. Ed.* **2022**, *61*, e202200666.

[11] a) J. Lyu, X. Zhang, P. Li, X. Wang, C. T. Buru, P. Bai, X. Guo, O. K. Farha, *Chem. Mater.* **2019**, *31*, 4166; b) J. Jia, L. Gutiérrez-Arzaluz, O. Shekhah, N. Alsadun, J. Czaban-Jóźwiak, S. Zhou, O. M. Bakr, O. F. Mohammed, M. Eddaoudi, *J. Am. Chem. Soc.* **2020**, *142*, 8580; c) W. Gong, X. Chen, W. Zhang, K. O. Kirlikovali, B. Nan, Z. Chen, R. Si, Y. Liu, O. K. Farha, Y. Cui, *J. Am. Chem. Soc.* **2022**, *144*, 3117.

[12] Y.-J. Hu, K. E. Knope, S. Skanthakumar, M. G. Kanatzidis, J. F. Mitchell, L. Soderholm, *J. Am. Chem. Soc.* **2013**, *135*, 14240.

[13] a) N. T. T. Nguyen, H. Furukawa, F. Gándara, C. A. Trickett, H. M. Jeong, K. E. Cordova, O. M. Yaghi, *J. Am. Chem. Soc.* **2015**, *137*, 15394; b) J. Chen, Q. Mei, Y. Chen, C. Marsh, B. An, X. Han, I. P. Silverwood, M. Li, Y. Cheng, M. He, X. Chen, W. Li, M. Kippax-Jones, D. Crawshaw, M. D. Frogley, S. J. Day, V. García-Sakai, P. Manuel, A. J. Ramirez-Cuesta, S. Yang, M. Schröder, *J. Am. Chem. Soc.* **2022**, *144*, 11969.

[14] L. Zhang, X. Liu, L. Li, D. Zhang, X. Sun, H. Yuan, *J. Alloys Compd.* **2018**, *743*, 136.

[15] a) J. Jiang, F. Gándara, Y.-B. Zhang, K. Na, O. M. Yaghi, W. G. Klemperer, *J. Am. Chem. Soc.* **2014**, *136*, 12844; b) T. N. Tu, N. Q. Phan, T. T. Vu, H. L. Nguyen, K. E. Cordova, H. Furukawa, *J. Mater. Chem. A* **2016**, *4*, 3638.

[16] E. Geravand, F. Farzaneh, M. Ghiasi, *J. Mol. Struct.* **2019**, *1198*, 126940.

[17] X.-M. Li, J. Liu, C. Zhao, J.-L. Zhou, L. Zhao, S.-L. Li, Y.-Q. Lan, *J. Mater. Chem. A* **2019**, *7*, 25165.

[18] J. Lin, N. Li, S. Yang, M. Jia, J. Liu, X.-M. Li, L. An, Q. Tian, L.-Z. Dong, Y.-Q. Lan, *J. Am. Chem. Soc.* **2020**, *142*, 13982.

[19] a) J. Wang, X. Yue, Z. Zhang, Z. Yang, Y. Li, H. Zhang, X. Yang, H. Wu, Z. Jiang, *Adv. Funct. Mater.* **2012**, *22*, 4539; b) P. Ramaswamy, N. E. Wong, G. K. H. Shimizu, *Chem. Soc. Rev.* **2014**, *43*, 5913.

[20] X. Liu, D. Zhang, L. Li, X. Sun, L. Zhang, H. Yuan, *Dalton Trans.* **2017**, *46*, 9103.

[21] a) S. S. Nagarkar, S. M. Unni, A. Sharma, S. Kurungot, S. K. Ghosh, *Angew. Chem., Int. Ed.* **2014**, *53*, 2638; b) X. Wang, F. Wang, C. Zhang, Q. Wang, *New J. Chem.* **2022**, *46*, 6657.

[22] P. J. Squattrito, P. R. Rudolf, A. Clearfield, *Inorg. Chem.* **1987**, *26*, 4240.

[23] S. Øien-Ødegaard, C. Bazioti, E. A. Redekop, Ø. Prytz, K. P. Lillerud, U. Olsbye, *Angew. Chem., Int. Ed.* **2020**, *59*, 21397.

[24] D. Leggas, O. V. Tsodikov, *Acta Crystallogr., Sect. A* **2015**, *71*, 319.

[25] O. V. Dolomanov, L. J. Bourhis, R. J. Gildea, J. A. K. Howard, H. Puschmann, *J. Appl. Crystallogr.* **2009**, *42*, 339.